Volume 10, Issue 3, 2020, 5400 -5405 ISSN 2069-5837
Biointerface Research in Applied Chemistry
www.BiointerfaceResearch.com
https://doi.org/10.33263/BRIAC103.400405
Original Research Article Open Access Journal
Received: 24.01.2020 / Revised: 02.03.2020 / Accepted: 05.03.2020 / Published on-line: 09.03.2020

Development of a high frequency piezoelectric immunosensor for the detection and quantification of BSA

Laura Buitrago [1], Camilo Ortiz [1], Kaory Barrientos [1], Marisol Jaramillo [1,*]
[1]Grupo de Investigación en Ingeniería Biomédica EIA, Universidad EIA, Calle 25 Sur 42-73 Envigado, Colombia, ZIP 055420
*corresponding author e-mail address: ***marisol.jaramillo@eia.edu.co*** | Scopus ID 55858131100

ABSTRACT
In this work, we developed a High Fundamental Frequency –Quartz Crystal Microbalance (HFF-QCM) immunosensor for the quantification of Bovine Serum Albumin (BSA) protein. Immobilization of BSA was achieved by means of mixed self-assembled monolayers (SAM), and we found that the largest phase shifts were produced with a concentration of 10 mg/mL. Then, we plotted an anti-BSA vs phase shift calibration curve, and obtained the analytical parameters that allowed us to compare our sensor to another anti–BSA QCM-based sensors. Our HFF-QCM immunosensor displays more sensitivity than low frequency QCM-based biosensors: its limit of detection (LOD) is 100 ng/mL and its linear range extends from 100 ng/mL to 5000 ng/mL. Finally, we fitted different adsorption isotherms models to our experimental data. We chose the Hill isotherm as it presented the highest coefficient of determination (R2), and we determined that the interaction between BSA and anti-BSA displays a positively cooperative binding behavior.
Keywords: *HFF-QCM; ATR-FTI; BSA; anti-BSA; Immunosensor; Isotherm.*

1. INTRODUCTION
Traditional biomolecule detection techniques are used in a range of fields such as in medicine [1] and the food industry [2], but their use requires many reagents and labeled molecules, as well as specialized equipment and qualified personnel [3, 4]. Biosensors are an alternative detection method that overcomes the limitations of traditional detection techniques, allowing real-time monitoring of biological events by transforming them into measurable signals [1]. To do this, they rely on two parts. The first part, or biological component, detects a biological event in a sample, and consists of a bioreceptor (that has a certain affinity for an analyte in a sample), and a biological interface (which hooks the bioreceptor to the surface of a transducer). Meanwhile, the second part, or transducer, transforms the biological event (derived from the interaction between the analyte and the bioreceptor) into a measurable signal. This makes it possible to detect and quantify an analyte in a sample [5]. When the detected biological event is the formation of immune complexes (that is, a specific antigen-antibody binding), the biosensor is called a piezoelectric immunosensor [6].

The natural oscillation frequency of a piezoelectric crystal working in QCM mode depends on the mass deposited on its surface. In 1959, Sauerbrey described the relationship between the observable shift in the resonance frequency of a crystal (Δf) and the mass deposited on its surface (Δm), as shown in Eq. 1 [7]:

$$\Delta f = -2 f_0^2 \Delta m / (\rho\mu)^{1/2} \quad \textbf{Eq. 1}$$

Where Δf is the frequency shift produced as a consequence of the mass alteration per unit of active area Δm, f_0 is the fundamental resonance frequency, ρ is the quartz density (2648 g/cm^3), and μ is the quartz shear modulus (29.47 dynes/cm^2, for AT-cut) [8].

Traditional QCM sensors exhibit an oscillation frequency that can range from 5 MHz to 20 MHz, but new high fundamental frequencies quartz crystal microbalances (HFF-QCM) display improved sensitivity [8]. In these high frequency transducers, the piezoelectric crystal must be interrogated with a signal at a constant frequency that is close to the natural frequency of the crystal —this allows measuring changes to the signal's phase. These changes are related to mass variations on the crystal's surface, as shown in Eq. 2 [9]

$$\Delta\varphi = \Delta m_s / m_L \quad \textbf{Eq. 2}$$

Where m_s is the surface mass density in contact with the crystal and m_L is the effect of the liquid displaced by the latter [10].

Only a number of researchers have used HFF-QCMs since their first application by Uttenthaler and colleagues in 2001 [11]: In 2015, March and colleagues developed a 100 MHz piezoelectric immunosensor for the detection and quantification of carbaryl, finding that its analytical performance surpassed that of conventional QCMs (it even got close to the standards of ELISA tests) [8]; Montoya and colleagues also used a HFF-QCM sensor in 2017, when they developed a 100 MHz piezoelectric immunosensor for the detection of a tuberculosis biomarker. Their immunosensor displayed higher sensitivity when compared with conventional QCMs —these results show promise for the detection of tuberculosis in biological fluids [10]. Given the interest of many researchers in highly sensitive QCM-based sensors and the promising results some have obtained, we expect research on new methodologies for the HFF-QCM-assisted detection of immune complexes to keep growing, starting with model measurements that can lay the ground for diagnostic applications. In this research, we developed an HFF-QCM piezoelectric immunosensor for the highly sensitive detection of anti-BSA (the specific antibody of model protein BSA). BSA (or Bovine Serum Albumin) is a plasmatic protein commonly used in biochemical and biosensing applications due to its binding properties, low cost, stability to increased signal during assays,

and lack of effect in many biochemical reactions; these reasons make it a convenient molecule to work with [12]. To develop our immunosensor, we first modified the surface of a quartz crystal gold electrode by means of mixed self-assembled monolayers (SAM). This allowed us to covalently attach the protein to the surface of the crystal and thus give way to antibody-antigen interactions. Then, to find the appropriate concentration of BSA to be used, we tested different concentrations of protein on the surface of 10MHz QCM transducers; the success of this process was confirmed via infrared spectroscopy. We also tested these concentrations on 100 MHz (HFF-QCM) transducers and picked the one that displayed the largest affinity. Finally, we obtained a calibration curve and analyzed our sensor's performance, comparing it to other authors.

2. MATERIALS AND METHODS

2.1. Reagents and instruments.

2.1.1. General.

Bovine Serum Albumin (98%) (BSA) and Anti-Bovine Serum Albumin (MOUSE) monoclonal antibody (anti-BSA) were obtained from Sigma-Aldrich (St. Louis, MO). BSA and anti-BSA were prepared by dissolving the corresponding concentrations in 0.1 M Phosphate Buffered Saline (PBS) pH 7.5, and PBST (PBS + 0.005% Tween 20), respectively. Tween 20 C58H114O26 was provided by Panreac (Barcelona, Spain). Carbaryl was donated by Universitat Politècnica de València (UPV). All other reagents were analytical grade.

2.1.2. Reagents for covalent immobilization.

Mercaptohexadecanoic acid $C_{16}H_{32}O_2S$ (90%) (MHDA) and 11-mercapto-1-undecanol $C_{11}H_{24}OS$ (97%) (MUD) were purchased from Sigma-Aldrich (St. Louis, MO). 1-ethyl-3 (-3 dimethyl-amino-propyl) carbodiimide hydrochloride $C_8H_{17}N_3HCl$ (EDC) and N-hydroxysuccinimide (NHS) were obtained from Thermo Scientific (Rockford, USA). Ethanolamine blocking agent C_2H_7NO was purchased from Sigma-Aldrich (St. Louis, USA).

2.1.3. Apparatus.

The 10 MHz QCM immobilized surfaces were characterized in an ATR-FTIR spectrophotometer by PerkinElmer. The 100 MHz immunosensor assays were performed in AWS A20-F20 test and flow platforms developed by AWSensors (Valencia, Spain, www.awsensors.com).

2.2. Quartz crystal microbalances.

2.2.1. HFF-QCM sensor chip and flow-cell assembly.

The 100 MHz transducers were obtained from AWSensors (Valencia, Spain). They consisted of AT-cut, inverted mesa quartz crystals with a total area of 36 mm^2 and an etched area thickness of approximately 17 µm. The gold electrode had an active surface of 0.785 mm^2 and a 1 mm diameter. The sensors were assembled on a polyether ether ketone (PEEK) support with a conical hole added to expose the active surface area of the electrode (so that it may contact the samples during the experimental assays). For their operation at high frequencies, the HFF-QCM chip was introduced in a flow cell, which allowed the crystal to make contact with the transducer and the flow system at the same time.

2.2.2. Measurement Platform.

The flow cell was mounted in the AWS A20 platform, which was connected to the AWS F20 module. The AWS A20 platform is an electronic characterization system in which the optimum operating frequency of the HFF-QCM is fixed, allowing phase shifts caused by events on the interface to be measured [13]. On the other hand, the AWS F20 module consists of a continuous flow system controlled by syringe pumps assisted remotely using the A20RP software. In this way, samples are delivered to the flow cell at a constant rate.

The A20RP software performs data acquisition and analysis. The optimum operation frequency (at which the sensor showed maximum conductance) was chosen via software. Phase, amplitude, and temperature measurements were taken, recorded, and processed throughout the assays.

2.2.3. 10 MHz QCM sensor.

The 10 MHz fundamental frequency AT-cut quartz sensors were obtained from ICM (Oklahoma, OK). These had a 13.67 mm blank diameter and a 5.11 mm Cr/Au electrode diameter (100 Å of Cr and 1000 Å of Au).

2.3. Surface modification.

2.3.1. 10 MHz QCM gold electrode surface functionalization and FTIR characterization.

Three different concentrations of BSA were covalently immobilized on the surface of the 10 MHz crystals. Infrared spectroscopy characterization was used to confirm the success of the process in every stage (SAM formation, SAM activation and BSA immobilization). Given that the 100 MHz crystals were fragile and the pressure of the spectrometer could easily break them, 10 MHz crystals were used instead. The procedures made on both crystals (10 and 100 MHz) were similar, the only differences being in the cleaning process and the composition of SAM.

The procedure was as follows: The crystals were cleaned for 5 min with 4 mL of Piranha solution (98% H_2SO_4 and 30% H_2O_2 at a 3:1 ratio), rinsed with bidistilled water and ethanol, and dried with nitrogen gas. Then, they were subjected to UV-ozone radiation for 20 min using a UV/Ozone ProCleaner (BioForce Nanosciences, USA), rinsed, and dried again. Covalent immobilization was carried out by means of classic amide chemistry to obtain mixed self-assembled monolayers (MSAM) of carboxylic alkane thiols as intermediate layers for protein binding. Procedures were performed following the protocol described by March [14], with a minor modification in the composition of SAM and in the protein. SAM consisted of a 10 mM mixed solution of MHDA and MUD (1:50 molar ratio), dissolved in ethanol. BSA protein solutions with concentrations of 10 mg/mL, 1 mg/mL and 0.1 mg/mL were prepared in PBS, and placed for 4 h on the previously activated crystals. Right after MSAM formed, they were activated with EDC and NHS, and BSA was immobilized. Then, the crystals were analyzed using FTIR spectroscopy. All samples were immobilized in duplicate.

2.3.2. HFF-QCM Gold electrode surface functionalization.

2.3.2.1. Selection of BSA concentration.

The 100 MHz crystals were cleaned and functionalized with SAMs (250 µM solution of MHDA and MUA in a 50:1 molar ratio) following the protocol described by March et al. [9]. After activation, three solutions of BSA (10 mg/mL, 1 mg/mL, and 0.1 mg/mL) were added and immobilized on the crystals to

find the most suitable concentration for the immunoassays. For this purpose, unlike in the March et al. protocol, we used in-flow protein immobilization. That is, the crystals were placed in the flow cell and then mounted on the measurement platform so that the samples could be pumped over the previously activated surfaces. This was done for 2 h while the phase shift measurements (caused by mass adsorption) were recorded. The assay had three steps:

- Baseline stabilization: working buffer flow (PBS) to stabilize the baseline signal.
- BSA flow (2 h).
- Baseline stabilization with the working buffer (20 min).

In all steps, a flow rate of 50 µL/min was used.

2.3.3. Immunoassay format in the HFF-QCM sensor.

A direct immunoassay was carried out on the HFF-QCM's surface to determine the response of the sensor to the formation of immune complexes (BSA and anti-BSA binding). For this reason, an optimal concentration of BSA (10 mg/mL) was immobilized on the functionalized crystals. BSA was immobilized by submerging the active surfaces in the protein solution for 5h under continuous stirring.

After BSA immobilization and prior to the first assay on every crystal, it was necessary to block the active sites where the protein did not bind, to prevent non-specific binding. Thus, a blocking buffer consisting of ethanolamine solution (10% v/v) in a 0.1 M sodium borate buffer (pH 8.75) was used. Then, the crystal was washed with sodium borate buffer and bidistilled water.

Then, by means of the AWS A20-F20 platforms, different concentrations of anti-BSA were pumped over the sensor. Solutions with concentrations of 30 µg/mL, 10 µg/mL, 5 µg/mL, 1 µg/mL, 0.5 µg/mL, and 0.1 µg/mL of anti-BSA were prepared in PBST. Then, 250 µl of each solution were laid on the functionalized surface. Variations in phase response were monitored in real time, as the binding between anti-BSA and immobilized-BSA occurred. Then, the functionalized surfaces were regenerated with 0.1 M HCl, to break the antigen-antibody interactions. Samples were run in duplicate (at least) and phase shift values were averaged for each concentration. Calibration curves were obtained by plotting the phase decrease vs. the analyte concentration. The experimental points were then fitted to the four-parameter logistic equation (Eq. 3):

$$f(x) = D + \frac{A - D}{1 + \left(\frac{x}{C}\right)^{B}} \qquad \textbf{Eq. 3}$$

Where, $f(x)$ is the HFF-QCM signal (variation of phase at the fixed fundamental frequency) produced by a given analyte concentration(x). A is the minimum asymptote. The $f(x)$ value in absence of analyte, B is the curve slope at the inflection point, C is the inflection point. C is the analyte concentration where $f(x) = (D - A)/2$, and D is the maximum asymptote (which can be considered as the $f(x)$ response value to an infinite analyte concentration).

3. RESULTS

3.1. 10 MHz QCM gold electrode ATR-FTIR characterization.

ATR-FTIR spectra confirmed the formation of SAMs. The bands at 2856 cm^{-1} and 2928 cm^{-1} (Figure 1a), attributed to symmetric and asymmetric vibrations of the methylene group (CH_2) in the backbone of SAMs, confirm their presence on the surface of the electrode. Characteristic bands of the alkanethiols, mainly at 1725 cm^{-1} (corresponding to carboxylic acids), and at 1465 cm^{-1} (related to the bending vibration of methylene groups), also appear in the spectra. In addition, the band at 1745 cm^{-1}, attributed to the NHS ester bond, evidences the success of the activation process. Finally, after immobilization of BSA (Figure 1b), two features appeared at 1550 cm^{-1} and 1663 cm^{-1}, assigned to the vibrations of amide II and I (which are present in most peptides) [15-17].

By monitoring all the stages of the process, we were able to verify the immobilization of the biomolecules. Bhadra et al. [18] used the same approach when they found characteristic bands at 2853 cm^{-1} and 2939 cm^{-1}, attributed to CH2 symmetric and asymmetric vibration modes; these bands are close to the ones shown in Figure 1a. They also observed peaks at 1745 cm^{-1} and 1849 cm^{-1} (which indicate the formation of NHS ester), and confirmed the immobilization of the protein with bands that appeared between 1500 cm^{-1} and 1700 cm^{-1}, specifically at 1604 cm^{-1} [18], analogous to Figure 1b. Thus, from this analysis, we expect BSA to have bonded to the surface of gold.

Figure 2 shows the FTIR spectra of the crystals after immobilization with 0.1 mg/mL, 1 mg/mL and 10 mg/mL BSA (in blue, orange, and gray, respectively). Bands around 1550 cm^{-1} and 1660 cm^{-1} (assigned to amide I and II, respectively) confirm the success of the process. On the spectra, we can observe how the largest concentration of protein (10 mg/mL) produces the strongest effect (deeper bands), followed by the intermediate concentration (1 mg/mL), and finally the smallest (0.1 mg/mL).

Thus, we can infer that greater concentrations of protein increase its accumulation on active sites.

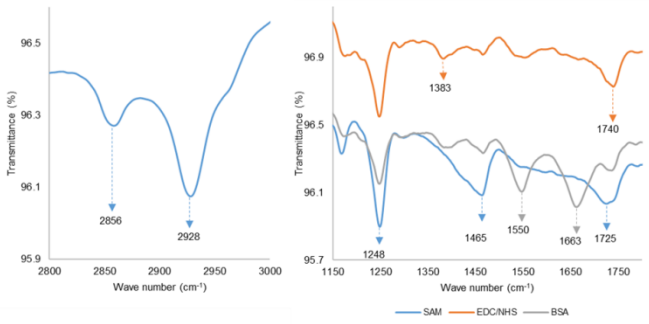

Figure 1. FTIR spectra of 10 MHz crystals after each immobilization stage. (a) FTIR spectra of MHDA and MUD terminated MSAM. Bands at 2856 and 2928 cm^{-1} are assigned to the symmetric and asymmetric methylene stretching bands from the MSAM backbone, respectively. (b) Stages of the immobilization process: MSAM, Activation and 10 mg/ml BSA immobilization (in blue, orange and gray, respectively).

3.2. Selection of BSA concentration.

To choose the concentration of BSA that allowed the largest quantity of protein bind to the active sites (on the 100 MHz crystals), we tested three concentrations of BSA dissolved in 0.1 M PBS (10 mg/mL, 1 mg/mL and 0.1 mg/mL). These were pumped for two hours over the previously functionalized crystals to ensure covalent immobilization of the protein, and then, we

recorded the phase shifts that arise due to the interaction between the samples and the surface.

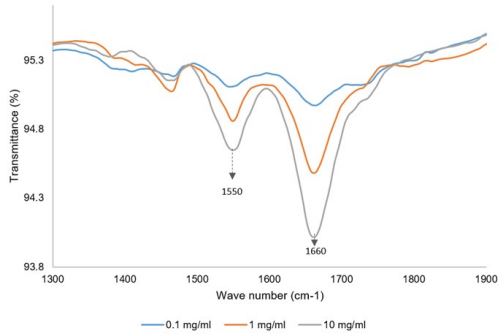

Figure 2. FTIR spectra (1300 – 1900 cm-1 region) of 10 MHz crystals after 0.1, 1 and 10 mg/mL BSA immobilization, in blue, orange and gray, respectively. Bands at 1661.03 and 1549.78 cm-1 correspond to the amide II and I vibrations, respectively, confirming the presence of the protein over the crystal surface.

Figure 3 shows the variation of the HFF-QCM signal (as a function of time) after interacting with 10 mg/mL BSA; the other two concentrations (1 mg/mL and 0.1 mg/mL) showed the same pattern: In region (I), the activated crystal was exposed to the working buffer until a steady baseline was obtained; in region (II), phase voltage began decreasing due to the flow of protein on the surface (2 h), until it later stabilized; in region (III), the BSA solution was replaced with the baseline solution (20 min). Each of the peaks in the figure appeared due to the suction caused by the syringe, as no substance flowed on the surface.

The recorded phase shifts were 0.525 V, 0.3 V, and 0.145 V (for the 10 mg/mL, 1 mg/mL and 0.1 mg/mL BSA concentrations, respectively). According to Eq. 2, changes in the signal's phase are directly proportional to the surface mass density in contact with the crystal. In that way, we expect the chosen concentration of protein to have caused the largest phase shift, as it retained the largest number of units bound to the active sites. For that reason, we chose 10 mg/mL for the immunoassay.

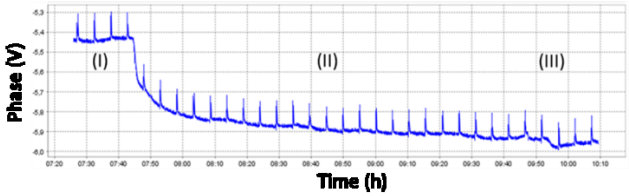

Figure 3. Molecular adsorption plot of the HFF-QCM signal phase change (V) vs time (h) for 10 mg/mL BSA adsorption onto the gold electrode of the 100 MHz crystal. Region (I): initial baseline solution, region (II): BSA flow (2 h), region (III): final baseline solution (20 min). 1 and 0.1 mg/mL BSA solutions showed this same plot pattern.

3.3. HFF-QCM standard curve.

Figure 4 shows the phase shifts produced by the antigen-antibody binding, and after regeneration of the crystal with HCl; the peaks between injections confirm these events. After regeneration, baseline was restored, suggesting antibody-antigen breakage. The interaction (binding events) took approximately 12 min. As expected of a direct immunoassay, higher concentrations (below the saturating concentration) produced larger phase shifts.

All signal variations followed the same pattern: as the immunocomplexes form (after injection of anti-BSA), the sensor's phase starts to decrease and then stabilizes after the crystal is exposed to the baseline solution.

To support these findings, we injected anti-carbaryl (the specific antibody for carbaryl) on the BSA-immobilized crystal and used it as a negative control. The baseline solution was PBST, and after anti-carbaryl injection, we observed no difference between the initial and final baseline phases, indicating anti-carbaryl failed to bind to the immobilized BSA. For this reason, we developed a specific piezoelectric immunosensor, as only anti-BSA can bind to BSA.

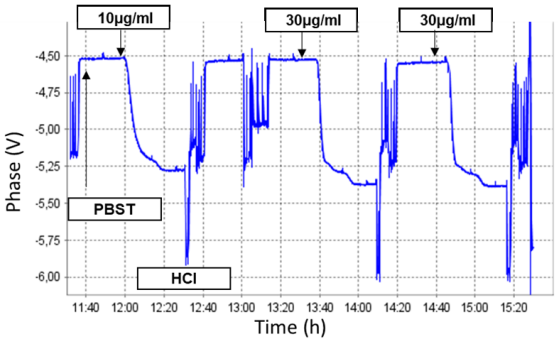

Figure 4. HFF-QCM immunosensor response to analyte concentration. Arrows indicate: baseline solution flow (PBST), which can be seen before each sample injection as a steady signal, sample injection (different concentrations of anti-BSA in PBST) and regeneration steps (HCl), which appear as high peaks.

After the immunoassay, we took the phase shifts we had recorded and produced a standard curve for the immunosensor (Figure 5). We averaged the phase shift values for each concentration, and then fitted the experimental data to a four-parameter logistic function, as shown in Eq. 3. In this study, we measured the sensitivity of the immunoassay by computing its linear range, slope, and limit of detection (LOD). We found a linear relationship between the phase shifts and the concentration of anti-BSA. Linear range was found to be between 0.1 µg/mL and 5 µg/mL, and the coefficient of determination R2 was equal to 0.9996; linear slope was 125.34 mV/ (µg/mL) and limit of detection (LOD) was 0.1 µg/mL —this limit is defined as the lowest anti-BSA concentration in the linear range that can alter the background signal (PBST).

3.4. Discussion.

In this research, we found that our high frequency sensor outperforms low frequency QCMs that use the same antibody-antigen pair: Szalontai's achieved a LOD of 1 µg/mL (10 times higher) [19].

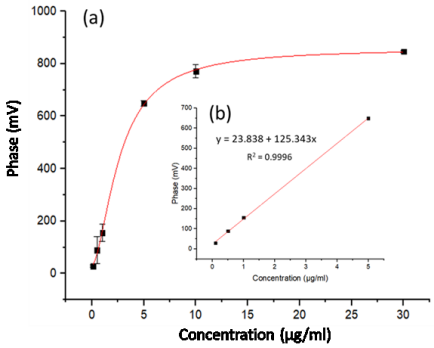

Figure 5. HFF-QCM BSA standard calibration curve, with phase shifts (mV) vs anti-BSA concentration (LOD = 0.1 µg/mL). Black squares represent the experimental points and error bars represent the standard deviation of the signal phase shifts. (b) Linear slope taken from the BSA standard calibration curve. The equation of the linear slope is shown, where "y" is the phase shift (mV) caused by mass adsorption and "x" is the anti-BSA concentration (µg/mL).

While comparing our sensor to other HFF-QCMs (March et al. [9] and Montoya et al. [11]) we found that, although the pattern of the calibration curve and the response of our sensor to the concentration of analyte matches the data in these studies, the analytical parameters differ; Table 1 shows a comparison of these parameters. Since the authors used different molecules (March et al. [9] used Carbaryl, Anti-Carbaryl and Montoya et. al [11] used 38 kDa, Myc-31), we expect the interactions between antibodies and antigens to differ and thus produce a different signal phase response. In addition, both authors produced specific monoclonal antibodies for their antigens, which could have provided greater afinnity. Finally, they both performed competitive assays, which might have also influenced the results.

Table 1. Comparison of the analytical parameters.

	HFF-QCM frequency	LOD (ng/mL)	WR (ng/mL)
March *et al.* [8]	100 MHz	0.14	0.26-1.73
Montoya *et al.* [10]	100 MHz	11	20-450
Present work	100 MHz	100	100-5000

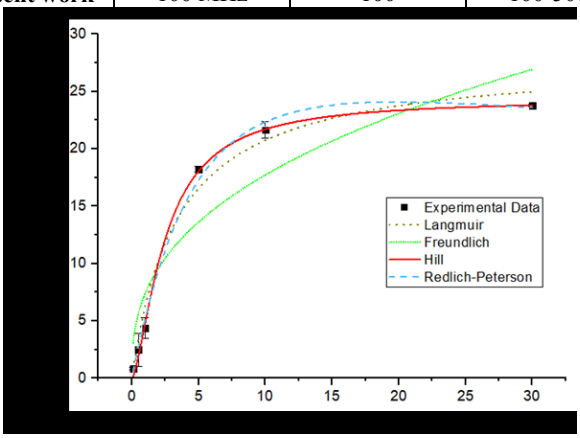

Figure 6. Non-linear regressions of different adsorption isotherms, with the amount of adsorbed BSA q_e (pg/mm2) vs anti-BSA concentration (µg/mL). Black squares represent the experimental points and error bars represent the standard deviation of the adsorbed BSA (q_e).

To describe the mechanism of immobilization, we used adsorption isotherms. As some authors have indicated, linearized models introduce a certain quantity of error, which does not permit a good fit to experimental data [20]. Thus, we employed non-linearized isotherms models to describe the behavior of adsorption. The best model was chosen based on its degree of fit (R2 value), is from lowest to highest: Freundlich, Langmuir, Toth, Redlich-Peterson and Hill; as shown in Figure 6.

The model that best fits the experimental data (Hill model) is given by Eq. 4.

$$q_e = (q_s {C_e}^n)/(K_D + {C_e}^n) \qquad \text{Eq. 4}$$

Where q_e is the amount of BSA that is adsorbed (pg/mm^2), C_e is the concentration of adsorbate at the equilibrium (µg/mL), q_e is the maximum specific uptake corresponding to the sites saturation (pg/mm^2), K_D is the Hill constant, and n is the Hill cooperativity coefficient. The last describes the degree of cooperativity between the subunits of a protein that binds a ligand [20,21]. Table 2 presents the parameters calculated for this work.

Table 2. Fitting parameters to the Hill isotherm for the BSA-anti-BSA system

Parameter	Value
q_S	24.35 ± 0.67
n	1.52 ± 0.12
K_D	4.05 ± 0.50
R^2	0.998

When constant n is larger than 1, cooperativity is said to be positive. In this work, we found there is a positive cooperative binding for anti-BSA after BSA immobilization. Some authors have worked with BSA - anti BSA pairings and found this behavior to be negative [22,23], but cooperativity may vary depending on the characteristics of the surface where the proteins are immobilized [24], or the ionic strength of the solvent used [25].

4. CONCLUSIONS

Immobilization of BSA on the 10 MHz sensors was characterized via ATR-FTIR. Bands at 1550 cm^{-1} and 1660 cm^{-1}, which suggest successful immobilization, were present on the spectra. In addition, phase shifts to the HFF-QCM signal were coherent with changes in the mass deposited on the sensor and indicated adhesion of the protein to the surface. Both events confirmed the success of immobilization, and showed how increasing concentrations of protein produce larger binding. For that reason, we decided on a concentration of 10 mg/mL.

Our HFF-QCM sensor is more sensitive than low frequency BSA/anti-BSA QCM-based sensors. We used a negative control to confirm the specificity of the sensor. This article suggests that this approach can be used in different antigen-antibody pairs, which could lead to many different applications.

The immobilization process was modeled by the construction of adsorption isotherms. Hill's model showed a better fit to the experimental data. The Hill coefficient (n) suggests anti-BSA binding with BSA displays a positively cooperative behavior

5. REFERENCES

1. Metkar, S.K.; Girigoswami, K. Diagnostic biosensors in medicine – A review. *Biocatalysis and Agricultural Biotechnology* **2019**, *17*, 271-283, https://doi.org/10.1016/j.bcab.2018.11.029.
2. Kobun, R.; Sulaiman, N.; Joseph, V.; Yi, S. Recent Biosensors Technologies for Detection of Mycotoxin in Food Products. In: *Mycotoxins and Food Safety*. 2019; https://doi.org/10.5772/intechopen.89022.
3. Wu, L.; Li, G.; Xu, X.; Zhu, L.; Huang, R.; Chen, X. Application of nano-ELISA in food analysis: Recent advances and challenges. *TrAC Trends in Analytical Chemistry* **2019**, *113*, 140-156, https://doi.org/10.1016/j.trac.2019.02.002.
4. Teleanu, D.M.; Chircov, C.; Grumezescu, A.M.; Volceanov, A.; Teleanu, R.I. Contrast Agents Delivery: An Up-to-Date Review of Nanodiagnostics in Neuroimaging. *Nanomaterials* **2019**, *9*, 542, https://doi.org/10.3390/nano9040542.
5. Cervera-Chiner, L.; Juan-Borrás, M.; March, C.; Arnau, A.; Escriche, I.; Montoya, Á.; Jiménez, Y. High Fundamental Frequency Quartz Crystal Microbalance (HFF-QCM) immunosensor for pesticide detection in honey.

Food Control **2018**, *92*, 1-6, https://doi.org/10.1016/j.foodcont.2018.04.026.
6. Skládal, P. Piezoelectric biosensors. *TrAC Trends in Analytical Chemistry* **2015**, *79*, https://doi.org/10.1016/j.trac.2015.12.009.
7. Sauerbrey, G. Verwendung von Schwingquarzen zur Wägung dünner Schichten und zur Mikrowägung. *Zeitschrift für Physik* **1959**, *155*, 206-222, https://doi.org/10.1007/BF01337937.
8. March, C.; García, J.V.; Sánchez, Á.; Arnau, A.; Jiménez, Y.; García, P.; Manclús, J.J.; Montoya, Á. High-frequency phase shift measurement greatly enhances the sensitivity of QCM immunosensors. *Biosensors and Bioelectronics* **2015**, *65*, 1-8, https://doi.org/10.1016/j.bios.2014.10.001.
9. Montagut, Y.J.; Garcia Narbon, J.; Jiménez, Y.; March, C.; Montoya, A.; Arnau, A. Frequency-shift vs phase-shift characterization of in-liquid quartz crystal microbalance applications. *The Review of scientific instruments* **2011**, *82*, https://doi.org/10.1063/1.3598340.
10. Montoya, A.; March, C.; Montagut, Y.J.; Moreno, M.J.; Manclus, J.J.; Arnau, A.; Jimenez, Y.; Jaramillo, M.; Marin, P.A.; Torres, R.A. A High Fundamental Frequency (HFF)-based QCM Immunosensor for Tuberculosis Detection. *Current topics in medicinal chemistry* **2017**, *17*, 1623-1630, https://doi.org/10.2174/1568026617666161104105210.
11. Uttenthaler, E.; Schräml, M.; Mandel, J.; Drost, S. Ultrasensitive quartz crystal microbalance sensors for detection of M13-Phages in liquids. *Biosensors and Bioelectronics* **2001**, *16*, 735-743, https://doi.org/10.1016/S0956-5663(01)00220-2.
12. Jahanban-Esfahlan, A.; Ostadrahimi, A.; Jahanban-Esfahlan, R.; Roufegarinejad, L.; Tabibiazar, M.; Amarowicz, R. Recent developments in the detection of bovine serum albumin. *International Journal of Biological Macromolecules* **2019**, *138*, 602-617, https://doi.org/10.1016/j.ijbiomac.2019.07.096.
13. Montagut, Y.; García, J.V.; Jiménez, Y.; March, C.; Montoya, A.; Arnau, A. Validation of a phase-mass characterization concept and interface for acoustic biosensors. *Sensors (Basel)* **2011**, *11*, 4702-4720, https://doi.org/10.3390/s110504702.
14. March, C.; Manclús, J.J.; Jiménez, Y.; Arnau, A.; Montoya, A. A piezoelectric immunosensor for the determination of pesticide residues and metabolites in fruit juices. *Talanta* **2009**, *78*, 827-833, https://doi.org/10.1016/j.talanta.2008.12.058.
15. Katrahalli, U.; Chanabasappa Yallur, B.; Manjunatha, D.H.; Krishna, P.M. BSA interaction and DNA cleavage studies of anti-bacterial benzothiazol-2-yl-malonaldehyde. *Journal of Molecular Structure* **2019**, *1196*, 96-104, https://doi.org/10.1016/j.molstruc.2019.06.062.
16. Wang, G.; Yan, C.; Gao, S.; Liu, Y. Surface chemistry of gold nanoparticles determines interactions with bovine serum albumin. *Materials Science and Engineering: C* **2019**, *103*, https://doi.org/10.1016/j.msec.2019.109856.
17. Arumugam, V.; Venkatesan, M.; Ramachandran, K.; Ramachandran, S.; Palanisamy, S.; Sundaresan, U. Purification, Characterization and Antibacterial Properties of Peptide from Marine Ascidian Didemnum sp. *International Journal of Peptide Research and Therapeutics* **2019**, https://doi.org/10.1007/s10989-019-09829-z.
18. Bhadra, P.; Shajahan, M.S.; Bhattacharya, E.; Chadha, A. Studies on varying n-alkanethiol chain lengths on a gold coated surface and their effect on antibody–antigen binding efficiency. *RSC Advances* **2015**, *5*, 80480-80487, https://doi.org/10.1039/C5RA11725A.
19. Szalontai, H.; Adányi, N.; Kiss, A. Development of Piezoelectric Immunosensor for the Detection of Probiotic Bacteria. *Analytical Letters* **2012**, *45*, 1214-1229, https://doi.org/10.1080/00032719.2012.673095.
20. Foo, K.Y.; Hameed, B.H. Insights into the modeling of adsorption isotherm systems. *Chemical Engineering Journal* **2010**, *156*, 2-10, https://doi.org/10.1016/j.cej.2009.09.013.
21. Abeliovich, H. An empirical extremum principle for the hill coefficient in ligand-protein interactions showing negative cooperativity. *Biophys J* **2005**, *89*, 76-79, https://doi.org/10.1529/biophysj.105.060194.
22. Zhou, L.; Wang, K.; Wu, Z.H.; Cheng, Z.L.; Bai, Y.N.; Zhou, H.B.; Jin, Q.H.; Mao, H.J.; Zhao, J.L. Heating induced self-assembly denatured Bovine serum albumin film on graphene targeting biomolecules. In: *2017 19th Int. Conf. Solid-State Sensors, Actuators Microsystems, IEEE*, 2017; pp. 1559–1562, https://doi.org/10.1109/TRANSDUCERS.2017.7994358.
23. Sansone, L.; Macchia, E.; Taddei, C.; Torsi, L.; Giordano, M. Label-free optical biosensing at femtomolar detection limit. *Sensors and Actuators B: Chemical* **2017**, *255*, https://doi.org/10.1016/j.snb.2017.08.059.
24. Janzen, R.; Unger, K.K.; Müller, W.; Hearn, M.T.W. Adsorption of proteins on porous and non-porous poly(ethyleneimine) and tentacle-type anion exchangers. *Journal of Chromatography A* **1990**, *522*, 77-93, https://doi.org/10.1016/0021-9673(90)85179-Y.
25. Luo, Q.; Andrade, J.D. Cooperative Adsorption of Proteins onto Hydroxyapatite. *Journal of Colloid and Interface Science* **1998**, *200*, 104-113, https://doi.org/10.1006/jcis.1997.5364.

6. ACKNOWLEDGEMENTS

The authors would like to extend their gratitude to Universidad EIA for the funding provided.